Effects of electron scattering at metal-nonmetal interfaces on electron-phonon equilibration in gold films

Patrick E. Hopkins,[a)] Jared L. Kassebaum, and Pamela M. Norris
Department of Mechanical and Aerospace Engineering, University of Virginia, P.O. Box 400746, Charlottesville, Virginia 22904-4746, USA

Electron scattering at interfaces between metals and dielectrics is a major concern in thermal boundary conductance studies. This aspect of energy transfer has been extensively studied and modeled on long time scales when the electrons and phonons are in equilibrium in the metal film. However, there are conflicting results concerning electron-interface scattering and energy transfer in the event of an electron-phonon nonequilibrium, specifically, how this mode of energy transfer affects the electron cooling during electron-phonon nonequilibration. Transient thermoreflectance (TTR) experiments utilizing ultrashort pulsed laser systems can resolve this electron-phonon nonequilibrium, and the thermophysical property relating rate of equilibration to electron-phonon scattering events G can be quantified. In this work, G in Au films of varying thicknesses are measured with the TTR technique. At large fluences (which result in high electron temperatures), the measured G is much larger than predicted from traditional models. This increase in G increases as the film thickness decreases and shows a substrate dependency, with larger values of G measured on more conductive substrates. The data suggest that in a highly nonequilibrium system, there could be some thermal energy lost to the underlying substrate, which can affect G. © *2009 American Institute of Physics*. [DOI: 10.1063/1.3068476]

I. INTRODUCTION

The occurrence of electron-phonon nonequilibrium in metal films is an important consideration in many nanoapplications. For example, a greater understanding of electron-phonon scattering and subsequent energy transport has made it possible for microelectronic engineers to develop field effect transistors that achieve high radio-frequency (rf) power levels in microwave radar and communications transmitter applications.[1] However, with these high rf power levels come extremely large thermal fluxes (>1 kW cm^{-2}) that can inhibit sufficient power dissipation away from active/heat generation regions causing self-heating, increased operation temperatures, and thermal cycling that degrade device gain and efficiency.[2] With the continued size reduction and increased operation frequencies envisioned in these devices, heat dissipation is becoming a growing challenge due to large resistances from electron-phonon coupling.[1,3,4] An added challenge is dealing with the thermal resistance from the electron-phonon nonequilibrium at the active layer/substrate interface. This electron-phonon nonequilibrium is also critical in, for example, advancement of ablation and laser machining of materials,[5–7] understanding spin dynamics in magnetic materials,[8–12] and further development of ultrashort pulsed laser systems.[13,14]

The thermal relaxation between the electron and phonon systems is efficiently observed with ultrashort pulsed laser techniques.[15] Electron-phonon nonequilibrium resulting from pulsed laser heating can be divided into three characteristic time intervals.[16,17] Consider an ultrashort laser pulse that is incident on the surface of a solid. The earliest of the time intervals, the length of which is termed as the relaxation time τ_{ee}, is typically of 10–100 fs for metals.[18] This time represents the time it takes for the excited electrons to relax into a Fermi distribution through electron-electron (e-e) collisions. These e-e collisions dominate electron-phonon (e-p) collisions during this time interval. Ballistic transport of the electrons also occurs during this time and the depth to which the electrons ballistically travel is significantly larger than the optical penetration depth in s- and p-band metals.[16,19] Once equilibrium is achieved within the electron system, the higher temperature electrons transmit energy to the lattice through e-p scattering processes as the electrons conduct energy deeper into the film away from the thermally excited region.[20,21] The e-p interactions eventually lead to the two subsystems reaching an equilibrium temperature within a time determined by the specific heats of the systems and the electron-phonon coupling factor.[15] This electron-phonon relaxation time τ_{ep} is typically on the order of 1 ps for metals and is inversely related to the electron-phonon coupling factor G,[22] which is typically on the order of 10^{16}–10^{17} W m^{-3} K^{-1} for metals.[16] Once e-p equilibrium is achieved, thermal transport is accurately described by the Fourier law as the thermal energy is transmitted deeper into the film at a rate proportional to the thermal conductivity of the material.

Electron-phonon relaxation at metal-nonmetal surfaces has been examined by several groups, mainly in imbedded-metal-nanoparticle geometries, with conflicting results.[23] For example, Arbouet *et al.*[24] found that electron-phonon relaxation time decreased (i.e., electron-phonon power transfer,

a)Present address: Engineering Sciences Center, Sandia National Laboratories, P.O. Box 5800, Albuquerque, NM 87185-0346. Electronic mail: pehopki@sandia.gov.

described by G, increased) as nanoparticle diameter decreased. Hodak *et al.*[25] extensively measured electron-phonon relaxation in Au nanoparticles and determined that the diameter of the nanoparticle had no effect on overall electron-phonon coupling. Hodak's analysis showed, however, that electron-acoustic surface mode interactions increased with a decrease in particle diameter, but the increase was minimal compared to the measured electron-phonon coupling in the particle.

There have been only a small number of studies looking at electron-phonon relaxation around interfaces in thin film systems. These studies avoid complications due to nanoparticle geometries (i.e., capillary modes) on determining the electron-phonon-interfacial interactions, and still, groups report conflicting results. Hohlfeld *et al.*[16] studied G in Au of various thicknesses for energies at and near the interband transition threshold (ITT) at two different incident laser fluences, −2.2 and 29 J m^{-2}, and measured the same G values as those measured during low-fluence intraband excitations by Smith and Norris,[26] −2.2×10^{16} W m^{-3} K^{-1}. Hohlfeld's study determined that at the specific probe energies around the ITT, no electron temperature or film thickness dependence was observed in G measurements in Au films. In addition, this study verified an enhanced thermal penetration depth in Au due to the large ballistic penetration depth, which is related to the large electron mean free path characteristic of the noble metals.[16,19] This observation allows for simplifying assumptions in the determination of G since large electron ballistic penetration depths presumably allow for G to be studied independent of any other variables in relatively thick films due to the lack of competing thermal diffusion processes which would complicate data analysis. Although Hohlfeld *et al.*[16] did not show a thickness or electron temperature dependence on electron phonon coupling factor in Au films, Bosco *et al.*[20] showed that *e-p* thermalization time can be affected by the substrate thermal conductivity. Bosco's study examined electron-phonon relaxation times in ultrathin NiFe films on NiO and Si substrates at a wide range of incident laser fluences and found that τ_{ep} increased with an increase in electron temperature. In addition, this study showed a substrate dependence in τ_{ep} which can be related to the effusivity of the substrate. Hopkins and Norris[27] showed an opposite temperature dependence in τ_{ep} than Bosco *et al.*[20] through electron-phonon coupling factor measurements in 20 nm Au films. This substrate dependence was not observed in the data of Hohlfeld *et al.*[16] most likely because the probe energy used during measurements of Hohlfeld *et al.*[16] was near the ITT energy. The thermoreflectance signal around the ITT is highly nonlinear and changes in optical reflectance associated with electron transitions around the ITT have been shown to influence electron-phonon thermalization measurements.[28] The different trends observed by Hopkins and Norris[27] and Bosco *et al.*[20] could be due to the different electronic band structures of Au and NiFe which lead to opposite electron-phonon coupling factor temperature dependencies due the different energies inducing *d*-band to *s*/*p*-band interband transitions.[29] Care must be exercised to take into account the effects of these transitions and the resulting reflectivity. This study examines electron-

phonon coupling factors in Au films in a specific transition regime to confidently extract the physics driving electron-interface and electron-phonon scattering during electron-phonon equilibration after short pulsed laser heating.

This paper examines the electron-phonon coupling factor of Au films of various thicknesses on Si and glass substrates measured with the pump-probe transient thermoreflectance (TTR) technique with a range of laser fluences. The pump-probe measurements are taken at 800 nm to only induce intraband transitions in the Au films, the temperature dependency of the reflectivity of which is well known.[26] In addition, the range of laser fluences is chosen to keep the electron temperature in a regime that does not cause any *d*-band thermal excitations.[29] A substrate dependency is observed in the measurements, which is attributed to electron-interface scattering during electron-phonon thermalization. This electron interface scattering, which drives thermal boundary conductance from the high temperature electron system, is quantified by comparing the measured electron-phonon coupling factor to that predicted from traditional models. This electron thermal boundary conductance during electron-phonon nonequilibrium is directly measured by fitting TTR data to the three temperature model.

II. THERMAL AND THERMOREFLECTANCE MODELS

A. Thermal model

The nonequilibrium temperature induced in the TTR experiments can be accurately predicted with the two temperature model (TTM).[18,30] This model, given by Eqs. (1) and (2), describes the rate of energy exchange between the electrons and phonons in a metallic film

$$C_e(T_e)\frac{\partial T_e}{\partial t} = \frac{\partial}{\partial x}\left(k_{\mathrm{eff}}(T_e,T_p)\frac{\partial T_e}{\partial x}\right) - G(T_e-T_p) + S(x,t),$$

(1)

$$C_p\frac{\partial T_p}{\partial t} = G(T_e-T_p),$$

(2)

where C_e is the temperature dependent electronic heat capacity defined as a product of the Sommerfeld constant γ and the electron temperature T_e,[31] G is the electron-phonon coupling factor,[32] C_p is the lattice heat capacity taken at 300 K,[33] which is assumed to be temperature independent due to minimal lattice heating during the few picoseconds after laser heating, and $k_{\mathrm{eff}}(T_e,T_p)$ is the effective electron thermal conductivity that accounts for *e-e* and *e-p* scatterings, defined as $k_{\mathrm{eff}}(T_e,T_l)=k_{eq}[T_e/T_p]$.[34] This expression for conductivity is valid for relatively low electron temperatures and is commonly used in TTM calculations.[6,15,26,28,32,35,36] However, when electron temperatures are driven above ~500 K, yet remain much lower than the Fermi temperature so the electron gas can still be considered degenerate, electron-electron scattering events will increase, which will decrease the conductivity from what is predicted from the previous simple expression for k_{eff}. Therefore, for temperatures much lower than the Fermi temperature, the more general expression for k_{eff} derived from kinetic theory should be used. This expres-

sion is given by[5] $k_{\text{eff}} = v_F^2 \gamma T_e / \{3(A_{ee}T_e^2 + B_{ep}T_p)\}$, where v_F is the Fermi velocity and A_{ee} and B_{ep} are electron-electron and electron-phonon scattering constants, respectively.[5,31,37,38] The energy transport processes modeled by the TTM are assumed one dimensional when the heated area is much greater than the film thickness. The laser source term $S(x,t)$ describes the radiation energy absorbed by the electron system and is given by[15]

$$S(x,t) = 0.94 \frac{(1-R)}{t_{\text{pulse}}R\left(1 - \exp\left[\dfrac{d}{R}\right]\right)}$$
$$\times J \exp\left[-\frac{x}{R} - 2.77\left(\frac{t - 2t_{\text{pulse}}}{t_{\text{pulse}}}\right)^2\right], \qquad (3)$$

where the film surface reflectivity R, film thickness d, and the energy penetration depth P are material properties, while the fluence J and the pulse duration t_{pulse} are parameters of the incident laser pulse. Here, P can be used to describe the sum of the radiation and ballistic penetration depths. The $(1 - \exp[d/P])$ expression ensures that all the laser energy absorbed by the electron system is contained in the electron system before electron thermalization, and not lost to the underlying substrate in the event that $d < P$. This term essentially imposes insulating boundary conditions to the electron system when $t < \tau_{ee}$, a time regime that the TTM is not suited to specifically analyze. Equations (1)–(3) are solved using the Crank–Nicolson method and insulative boundary conditions are typically appropriate.[22]

B. Thermoreflectance models

In TTR experiments, it is the change in reflectivity ΔR resulting from a change in temperature in the sample that is measured. The change in reflectance of a metal can be related to the change in temperature through the change in the complex dielectric function $\Delta\varepsilon(\omega, \Delta T) = \Delta\varepsilon_1(\omega, \Delta T) + i\Delta\varepsilon_2(\omega, \Delta T)$, where $\Delta\varepsilon_1(\omega, \Delta T)$ and $\Delta\varepsilon_2(\omega, \Delta T)$ are the changes in the real and imaginary parts of the complex dielectric function, respectively.[39] For ultrashort pulses ($\tau_{ee} < t_{\text{pulse}} < \tau_{ep}$), the resulting reflectance, and thus the dielectric function, is a function of both ΔT_e and ΔT_P: $\Delta\varepsilon(\omega, \Delta T_e, \Delta T_P) = \Delta\varepsilon_1(\omega, \Delta T_e, \Delta T_P) + i\Delta\varepsilon_2(\omega, \Delta T_e, \Delta T_P)$. For small changes in temperature ($\Delta T_e, \Delta T_p < 150$ K), $\Delta\varepsilon$ can be expressed as a linear change in ΔT_e and ΔT_p,[15,40,41]

$$\Delta\varepsilon = \Delta\varepsilon_1 + i\Delta\varepsilon_2 = \frac{\partial\varepsilon_1}{\partial T_e}\Delta T_e + \frac{\partial\varepsilon_1}{\partial T_p}\Delta T_p$$
$$+ i\left(\frac{\partial\varepsilon_2}{\partial T_e}\Delta T_e + \frac{\partial\varepsilon_2}{\partial T_p}\Delta T_p\right), \qquad (4)$$

where the functional dependence of ε is dropped for clarity. The change in reflectance in TTR experiments can be related to the dielectric functions by[42]

$$\frac{\Delta R}{R} = \frac{1}{R}\left[\frac{\partial R}{\partial\varepsilon_1}\Delta\varepsilon_1 + \frac{\partial R}{\partial\varepsilon_2}\Delta\varepsilon_2\right]. \qquad (5)$$

By plugging Eq. (4) into Eq. (5), the reflectance can be simplified to the familiar thermoreflectance equation[15,40]

$$\frac{\Delta R}{R} = a\Delta T_e + b\Delta T_p, \qquad (6)$$

where $a \propto \partial R/\partial T_e$ and $b \propto \partial R/\partial T_p$. This reflectance model directly relates the change in reflectance in TTR experiments to the electron and phonon temperatures in the TTM. The coefficient a is determined by fitting the peak of the electron temperature profile in the TTM to the peak of the TTR data, and the coefficient b is determined by fitting the lattice temperature profile at some time after the electron peak when the electron and phonon systems are in equilibrium.[15,40] Once the change in temperatures of the electron and lattice systems are extracted from the experimental TTR data, this information can be used to determine thermophysical properties such as the electron-phonon coupling factor by fitting the TTM to the TTR data using G as a free parameter to minimize error.[36] This is discussed in more detail in Sec. III.

The thermoreflectance model presented in Eq. (6) is dependent on the fact that ΔT_e and $\Delta T_p < 150$ K. This is easy to ensure in metals with relatively high Sommerfeld constants, but in metals with low Sommerfeld constants, such as the noble metals, very low incident laser fluences will lead to large changes in electron temperature yielding Eq. (6) inapplicable. However, noble metals have a very distinct, high energy ITT since the s-band/d-band crossing is significantly lower than the Fermi level. The lowest energy d-band to available Fermi level transition is very large for Cu (2.15 eV), Au (2.4 eV), and Ag (4 eV), making it easy to isolate the effects of the interband and intraband transitions on thermoreflectance.[43] Transition metals, in contrast, pose a greater problem in isolating the various transitions and determining their dependencies on G through TTR since characteristically, transition metal band structures are shifted from the noble metals so the s-band/d-band crossing is at or above the Fermi level. This produces several allowable low energy d-band (d_1-band) to s-band transitions making it difficult to examine the relative effects of inter- and intraband transitions. For example, Cr has Fermi transitions at 0.8 (ITT), 1.0, 1.4, and 1.6 eV, W has transitions at 0.85 (ITT), 1.6, and 1.75 eV,[44] and Ni has transitions at 0.25 (ITT), 0.4, and 1.3 eV.[45]

In terms of the thermoreflectance model, this high energy ITT in noble metals can lead to significant simplifications. This is apparent in the nature of the complex dielectric function ε. It has been shown that the change in the complex dielectric function can be expressed as $\Delta\varepsilon = \Delta\varepsilon^{(f)} + \Delta\varepsilon^{(b)}$ which separates the intraband effects [free electron effects denoted by the superscript (f)] from interband effects [bound-electron effects denoted by the superscript (b)] explicitly.[46,47] Both $\Delta\varepsilon^{(f)}$ and $\Delta\varepsilon^{(b)}$ are complex expressions with real and imaginary parts. Therefore, $\Delta\varepsilon$ can be rewritten in the form of Eq. (4) as $\Delta\varepsilon = \Delta\varepsilon_1 + i\Delta\varepsilon_2$, where $\Delta\varepsilon_1 = \Delta\varepsilon_1^{(f)} + \Delta\varepsilon_1^{(b)}$ and $\Delta\varepsilon_2 = \Delta\varepsilon_2^{(f)} + \Delta\varepsilon_2^{(b)}$.

Now consider an example of a metal irradiated with photons where the incident photon energy is less than the ITT,

TABLE I. Properties used in TTM calculations for Au films.

γ [W m^{-3} K^{-2}]	k_{eq} (W m^{-1} K^{-1})	G (W m^{-3} K^{-1})	C_p (J m^{-3} K^{-1})	t_{pulse} (fs)	$n_{1,\mathrm{Au}}$	$n_{2,\mathrm{Au}}$	$n_{1,\mathrm{Si}}$	$n_{2,\mathrm{Si}}$
71.4	317	2.2×10^{16}	2.5×10^{6}	100	0.18	5	3.692	0.0065

R 30 nm Au/Si	R 30 nm Au/SiO$_2$	R 50 nm Au/Si	R 50 nm Au/SiO$_2$	P_o (nm)	P (nm)	$n_{1,\mathrm{SiO_2}}$	$n_{2,\mathrm{SiO_2}}$	$n_{1,\mathrm{air}}$
0.84	0.88	0.94	0.95	12.5	120	1.454	0	1

i.e., $\hbar\omega <$ ITT. In this case, the change in reflectance of the metal is dominated by the intraband transitions from the free electrons (since there is not enough energy in the incident photons to excite the bound electrons to undergo an interband transition). Therefore, $\Delta\varepsilon = \Delta\varepsilon^{(f)}$. The change in the free electron dielectric function with temperature for this metal is described by the change in the free electron, or Drude model, given by[48–50]

$$\varepsilon^{(f)} = 1 - \frac{\omega_{\mathrm{plasma}}^2}{\omega(\omega + i\omega_\tau)} = 1 - \frac{\omega_{\mathrm{plasma}}^2}{(\omega^2 + \omega_\tau^2)} + i\frac{\omega_\tau\omega_{\mathrm{plasma}}^2}{\omega(\omega^2 + \omega_\tau^2)}, \quad (7)$$

where ω is the frequency of the incident photons, ω_{plasma} is the plasma frequency of the free electrons, and ω_τ is the collisional frequency of free electrons excited by the incident photons. In order to relate the change in the dielectric function, and therefore the change in reflectance, to the change in electron and phonon temperatures, and therefore relate TTR data to the TTM, the temperature dependence of ω_τ must be exploited. This collisional frequency is inversely proportional to electron collisional time, and therefore Matthiessen's rule[51] can be used to express the free electron collisional frequency as[38] $\Delta\omega_\tau = 1/\Delta\tau \approx A_{ee}\Delta T_e^2 + B_{ep}\Delta T_p$, where A_{ee} and B_{ep} are the material constants relating to the temperature dependencies of the electron-electron and electron-phonon collisional frequencies, as previously mentioned.[5,31,37,38]

Smith and Norris[26] exploited the relationship between the metal's reflectivity and the dielectric function to derive a thermoreflectance model that explicitly takes into account the change in electron and phonon temperatures during intraband transitions, which is reviewed here. The reflectivity of a solid is calculated by the well known relationship[52]

$$R = \frac{(n_1 - 1)^2 + n_2^2}{(n_1 + 1)^2 + n_2^2}, \quad (8)$$

where n_1 and n_2 are the real and imaginary parts of the index of refraction n, which, in the case of intraband excitations only, is related to the complex dielectric function by $n = n_1 + in_2 = \sqrt{\varepsilon^{(f)}}$. The real and imaginary parts of n can be found in tables of the optical properties of materials.[53] However, given a change in electron and phonon temperatures, the change in n_1 and n_2 can be evaluated, and the change in reflectivity ΔR can be calculated. $\Delta R/R$ is calculated by dividing ΔR by Eq. (8), since Eq. (8) gives the baseline reflectivity at a given temperature, and ΔR determines how much this baseline reflectance changes as a result of changes in electron and phonon temperatures. The fitting procedure of

this intraband reflectance model is similar to that of the standard reflectance model in Eq. (6). In this case, however, the change in electron temperature is related to the change in reflectance via $\Delta\omega_\tau$. The change in phonon temperature is still considered linearly related to the change in reflectance as in Eq. (6) since the change in lattice temperature is minimal in the cases considered here.

The intraband reflectance model[26] gives the explicit electron and phonon temperature dependence of the change in reflectivity of a film undergoing intraband transitions valid for all temperatures. In the event that interband transitions are excited and contributing to the thermoreflectance, Eq. (6) must be used, and its small change in temperature restriction must be adhered to. The remainder of this work will focus on nonequilibrium heating in Au when intraband transitions dominate the thermoreflectance. As previously mentioned, Au has been extensively studied, so the data presented in this work have a large database of previous studies for comparison. In addition, the intraband reflectance model allows for electron-phonon coupling in Au to be studied at relatively high fluences that induce changes in the electron temperatures of thousands of degrees Kelvin.

Although the intraband reflectance model is suited to study electron-phonon nonequilibrium at high electron temperatures, in the event that the film thickness is approximately the same as the optical penetration depth, $P_o = \lambda/4\pi n_2$, where λ is the wavelength of the incident photons, the reflectivity on the surface of the film is affected by the substrate, and therefore, the standard reflectivity equation given by Eq. (8) must be modified to take into account the optical properties of the substrate. Consequently the intraband reflectance model must be modified. The Au films in this study are grown on Si and SiO$_2$ substrates, both of which have very low values for n_2, the imaginary part of n, as given in Table I. This parameter is called the extinction coefficient and indicates the optical absorption of a material. Therefore, the reflectivity of the Au/substrate samples examined in this work can be calculated with the equation for reflectivity of an absorbing film on a nonabsorbing substrate, derived by Abeles.[54] Figure 1 shows the predicted $\Delta R/R$ of the thickness dependent intraband reflectance model derived by Smith and Norris[26] for 30 and 50 nm Au films on Si and SiO$_2$ substrates as a function of electron temperature while assuming the phonon temperature is held constant at 300 K. The nonlinearity with temperature and variability with film thickness are apparent. The inset of Fig. 1 shows the reflectivity at 300 K for Au/Si and Au/SiO$_2$ as a function of film thickness
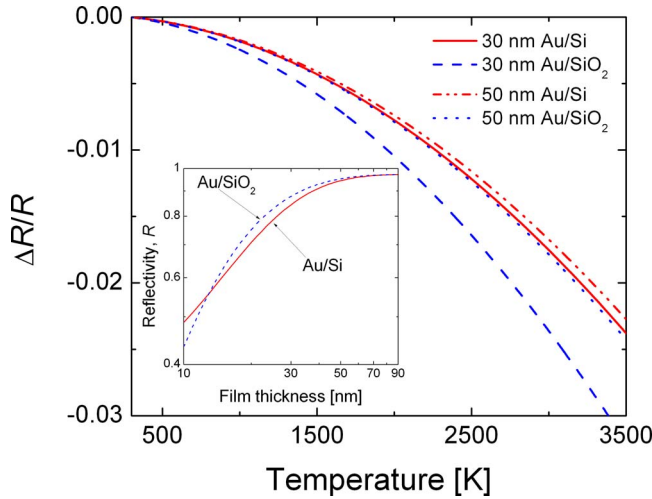
FIG. 1. (Color online) $\Delta R/R$ predictions from the thickness dependent intraband reflectance model derived by Smith and Norris (Ref. 26). The nonlinearity and substrate dependency are apparent showing that at high temperatures and thin films, this model must be used as opposed to Eq. (6) when only intraband transitions are induced. The inset shows the equilibrium reflectance R off the surface of an Au film on both Si and SiO$_2$ substrates as a function of film thickness at a wavelength of 800 nm (1.55 eV). For films thinner than 50 nm, the reflectance deviates by more than 10% from the bulk reflectance, indicating that for films in this range the absorbed laser energy in TTR experiments could be affected by the underlying substrate.

FIG. 2. (Color online) Phase corrected TTR data on 30 and 50 nm Au/glass samples taking with 15 J m^{-2} incident laser fluence. The data are normalized at the peak reflectance to show the difference in cooling profiles of the electron systems after laser heating. The initial time (t_0) is defined at the time of peak reflectance. The inset shows the calculations of the TTM, assuming homogeneous heating [Eqs. (9)–(11)] fit to the first 2.0 ps of the data after laser heating. The best fit resulted in different G for the two laser fluences.

d. These calculations assume an incident wavelength of λ =800 nm (1.55 eV), the values for n_1 and n_2 listed in Table I for air, Au, Si, and SiO$_2$,[53] and A_{ee} and B_{ep} for Au as 1.2 $\times 10^7$ K^{-2} s^{-1} and 1.23$\times 10^{11}$ K^{-1} s^{-1}, respectively.[37,55,56] Note that in Au, A_{ee} and B_{ep} are temperature independent.[57] The formulation of the intraband thermoreflectance model[26] using the film thickness reflectivity relations is suited to relate ΔR to any ΔT in a film of any thickness in the event that intraband transitions dominate the TTR response.

III. ELECTRON-PHONON AND ELECTRON-INTERFACE SCATTERINGS IN AU FILMS

This study presents the measurements of the electron-phonon coupling factor of Au films of varying thicknesses on Si and SiO$_2$ substrates with the goal of examining potential film thickness or fluence dependency. Assuming an insulated film system, the change in film thickness and fluence will alter the electron and phonon temperatures in such a way that can be predicted by theory. To test this, Au films of 30, 40, and 50 nm of thickness were sputter deposited on Si and SiO$_2$ substrates and G was determined using the same short-pulsed TTR technique and parameters described by Hopkins and Norris.[27] The 30, 40, and 50 nm Au samples were subjected to 10 and 15.0 J m^{-2} incident laser fluence. Seven to ten TTR measurement scans were taken on each Au sample.

Phase corrected TTR data[58] for the 30 and 50 nm Au/glass film taken at 15 J m^{-2} incident laser fluence are shown in Fig. 2. These data are normalized at the peak reflectance to observe the difference between the electron cooling profiles at these different fluences, and $t=0$ is defined as the time at maximum reflectance. It is the shape of the cooling profile after the maximum electron temperature that is related to the rate of electron-phonon equilibration; therefore, the normal-
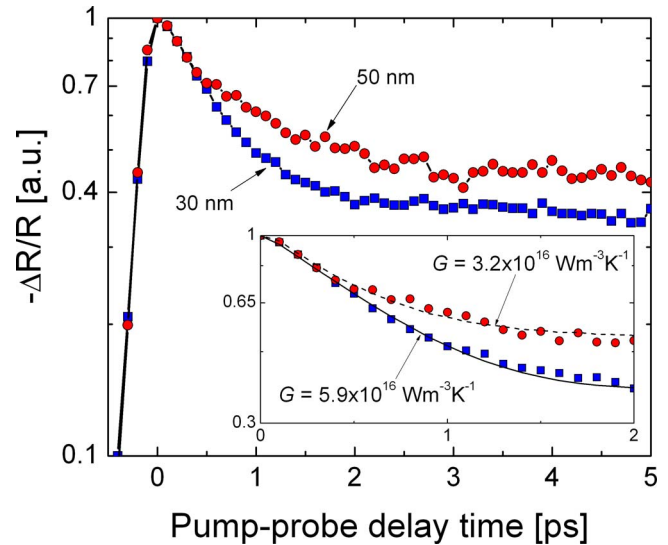
ization of the data is for clear comparison between the two data sets. The majority of the electron energy loss to the phonons occurs within 1–2 ps after laser heating. Differences in the data are seen within 2 ps after the maximum reflectance, indicating a difference in the cooling rate of the electron system during electron-phonon equilibration.

In order to determine G from the TTR measurements, $\Delta R/R$ from the TTR data is related to the change in temperature predicted from the TTM with the thickness dependent intraband thermoreflectance model discussed in the previous section and the thermophysical parameters in Table I. The energy penetration depth in a material can be estimated by $P = \sqrt{k_{eq}/G}$, which gives 120 nm in Au at room temperature.[21] This represents the distance to which the excited carriers (in this case, electrons) penetrate into the film before relaxing into a thermal distribution ($t < \tau_{ee}$). This can also be thought of as the distance an electron travels before experiencing a collision that redistributes the electron energy, which statistically is represented by the mean free path Λ. From kinetic theory,[59] $\Lambda = 3k_{eq}/(C_p v_L) \approx 115$ nm for Au, in good agreement with P, where v_L is the longitudinal phonon velocity (electron velocity during diffusive transport) taken as 3300 m s^{-1}.[55] This thermal penetration depth was also observed experimentally in Au films.[16] The Au samples in this study are thinner than this energy penetration depth d $< P$, and therefore the electrons penetrate the entire thickness of the film before colliding and relaxing into an equilibrium thermal Fermi distribution. Therefore, the Au films are assumed to be homogeneously heated after τ_{ee}, meaning the electron temperature difference between the front and rear surfaces of the film can be assumed negligible ($\partial T_e / \partial x$ =0).[16] Therefore, the TTM can be re-expressed as

$$C_e(T_e)\frac{\partial T_e}{\partial t} = -G(T_e - T_p) + S(t), \tag{9}$$

$$C_p\frac{\partial T_p}{\partial t} = G(T_e - T_p), \tag{10}$$

$$S(t) = 0.94\frac{(1-R)J}{t_{pulse}d}\exp\left[-2.77\left(\frac{t-2t_{pulse}}{t_{pulse}}\right)^2\right], \tag{11}$$

and an appropriate choice of the film thickness d ensures that all the incident laser energy is absorbed in the electron system. Using the film thickness d as the characteristic length in which the incident fluence is absorbed in the film is appropriate when $d < P$ and assumes that some degree of ballistic transport will be blocked and reflection at the film/substrate boundary results in a higher energy density within the film.[16] This calculation assumes total reflection of the electron energy back into the depth of the film with spatial homogeneity. Using the exact film thickness d in Eq. (11) is a slightly more exact expression than $P(1-\exp[d/P])$ in Eq. (3) and can be used when $d < P$. Note that $P(1-\exp[d/P])$ is meant to reduce to d when $d < P$.

With the intraband thickness dependent reflectance model discussed in Sec. II, Eqs. (9) and (10) are fit to the first 2.0 ps of data immediately following the transient peak and G is treated as a free parameter to attain the minimum error. This corresponds to the time when the majority of the e-p coupling occurs; however, excellent agreement between the model and the data is observed for several picoseconds after the peak. The best fit G is obtained at the minimum error between the data and the fit, typically less than 1% in this study.

The inset of Fig. 2 shows the TTM fit to experimental data with the best fit values for G as determined from TTR data taken on both the 30 and 50 nm samples. These data show noticeably different cooling profiles with the only variation between the measurements being the film thickness. On the 50 nm Au/glass sample, G was determined to be 3.2×10^{16} W m^{-3} K^{-1}, yet the best-fit value of G measured in the 30 nm Au/glass sample was almost a factor of two larger, 5.9×10^{16} W m^{-3} K^{-1}.

The increased laser fluence causes an increase in electron temperature which creates a subsequent increase in G, as predicted by Chen et al.[60] The predicted maximum electron temperature on the 30 nm Au/glass sample associated with the 15 J m^{-2} incident fluence in Fig. 2 (along with the experimentally determined value of the e-p coupling factor, 5.9×10^{16} W m^{-3} K^{-1}) is ~1943 K. At this temperature, G is predicted as 2.5×10^{16} W m^{-3} K^{-1} with the model of Chen et al.[60] assuming a room temperature G of 2.2×10^{16} W m^{-3} K^{-1};[60] this predicted value is significantly less than the measured G.

Figure 3 shows the values of G measured on 20, 30, 40, and 50 nm Au/glass and Au/Si samples, as predicted by the TTM best fit with 10.0 and 15.0 J m^{-2} fluences as a function of film thickness. The 20 nm data were taken from Hopkins and Norris.[27] As the Au films increase in thickness, the incident laser energy absorbed by the electron system is stretched out among a greater film depth, thereby decreasing
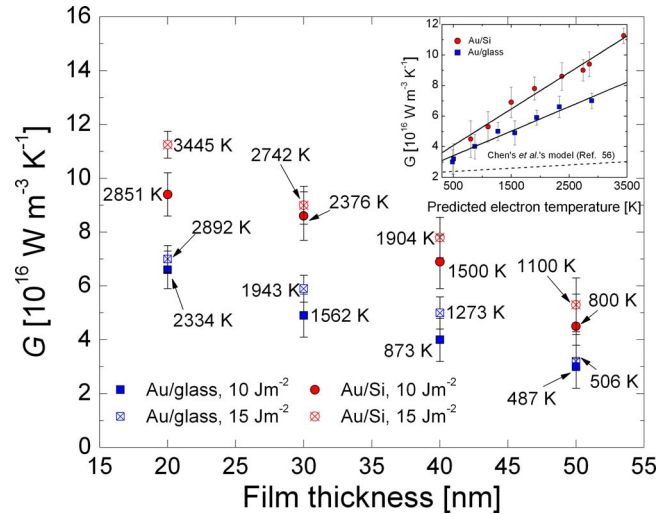

FIG. 3. (Color online) Best fit G measured on eight different Au samples using 10 and 15 J m^{-2} incident laser fluence. Associated with each data point is the corresponding maximum electron temperature determined from the TTM fit. As temperature decreases, the measured G also decreases, yet the trends of G with temperature show different dependencies depending on the substrate, showing evidence of substrate interference in electron-phonon equilibration. The 20 nm data are from Hopkins and Norris (Ref. 27). The inset recasts the measured G on the different samples as a function of predicted maximum electron temperature achieved after pump absorption predicted by the TTM. The different trends between the measured data and G predicted with the model of Chen et al. (Ref. 60) suggest that scattering at the film/substrate boundary is affecting G measurements. The difference between the Au/Si and Au/glass measurements suggests that the properties of the substrate also affect G measurements.

the energy density in the electron system. This results in a decrease in the measured G, yet still, there is a discrepancy between G measured on the different substrates. This could be a result of high temperature electrons at the film/substrate boundary losing energy through electron-boundary scattering, thereby offering another mechanism of energy loss from the electron system. In the thermally conductive substrate Si, the thermal energy is more readily transferred from the Au electron system to the substrate than in the thermally insulative substrate glass. The error bars associated with each data point represent the standard deviation from the multiple TTR scans taken at each fluence on each sample. Note that the deviation from the mean increases as the samples get thicker. This is due to the fact that there is less substrate interference in the film reflectance as the film gets thicker, and therefore less of the incident fluence is absorbed (Fig. 1). This causes a smaller thermoreflectance signal from the Au surface since the Au electrons are not reaching as high of a temperature, and therefore the signal to noise ratio from the Au thermoreflectance data decreases. This caused a greater deviation from the mean G determined by the fitting procedure outlined above.

The inset of Fig. 3 recasts the measured G and G_{meas} as a function of predicted maximum electron temperature. As the Au film gets thinner and the magnitude of the electron-phonon nonequilibrium at the film/substrate interface increases, the difference between G_{meas} and G predicted by the model of Chen et al.[60] becomes more pronounced. The differing temperature trends and values of G_{meas} between the Au/Si and Au/glass samples, which also differ from what is

expected in Au at the given electron temperature via the model of Chen *et al.*,[60] suggest that electron-interface scattering is dependent on properties of the underlying substrate. If G_{meas} was only dependent on electron and phonon film temperatures, then results for the Au/glass and Au/Si samples would not diverge at high temperatures. However, the differing high temperature trends between the samples indicate that some properties of the boundary (which would differ based on differing properties between Si and SiO$_2$) could be affecting the measurements. The rate at which the G measurements increase with temperature is much greater in the Au/Si sample than the Au/glass sample, which could be due to the differing thermal properties of the substrate. This is conceptually intuitive since a thermally conductive substrate like Si would be more apt to transfer energy away from the electron system than an insulating substrate like glass. The higher the electron temperature, the greater the rate of energy transfer between the electron system and substrate through electron-boundary scattering, thereby increasing the apparent electron-phonon coupling factor as determined with the TTR technique. As previously mentioned, these trends were not seen by Hohlfeld *et al.*[16] who examined Au films at various fluences around the ITT. However, this channel of electron-substrate energy transfer could in fact still be present in their data but the large optical response associated with the interband transition could mask any effects of the free electron gas loosing energy to the underlying substrate.[28]

In order to quantify electron-substrate scattering from TTR data, the TTM must be modified to take into account electron-substrate energy transfer h_{es}. Hopkins and Norris[27] used a three temperature model to quantify this energy pathway in 20 nm Au films given by

$$C_e(T_e)\frac{\partial T_e}{\partial t} = -G(T_e - T_p) - \frac{h_{es}}{d}(T_e - T_0) + S(t). \quad (12)$$

To predict h_{es}, Eq. (12) is fit to the TTR data using h_{es} as a free parameter until a best fit G is achieved that matches G predicted via the model of Chen *et al.*[60] The resulting h_{es} determined from the Au/Si and Au/glass TTR data is shown in Fig. 4. The measured h_{es} increases over the range of predicted electron temperatures, with h_{es} increasing more rapidly with temperature on the Si substrate than the glass substrate, indicating a substrate dependence on electron-phonon equilibration. However, the thermal conductivity is over two orders of magnitude greater than the thermal conductivity of glass. In fact, glass is a very poor thermal conductor. Therefore, it is not expected that the glass substrate will act as a heat sink that will cause a significant amount of electron energy to transfer out of the film during nonequilibrium heating. The increase in h_{es} observed in the Au/glass samples is most likely due to electron-interface scattering at the film/substrate boundary, which could be facilitated by impurities and other defects introduced during the deposition process. Although a disordered region is still expected at the Au/Si interface, additional energy is conducted away from the high temperature scattered electrons due to the high thermal conductivity of Si. Therefore, h_{es} measured on Au/glass represents the effects of the high temperature Au electrons loosing energy by scattering at an interface of two materials, and the
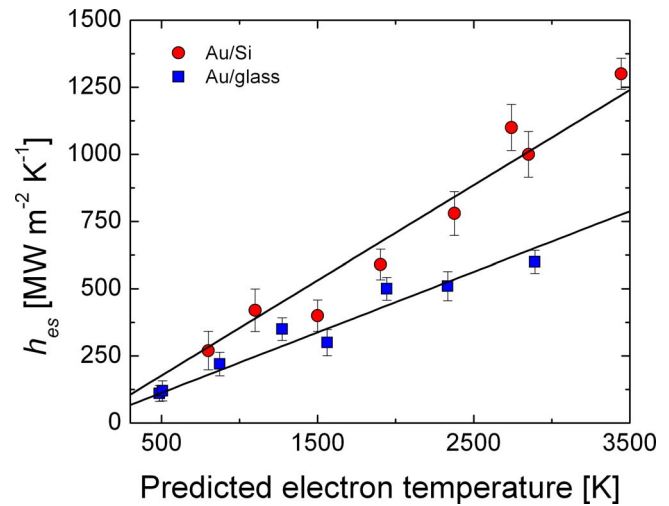

FIG. 4. (Color online) h_{es} determined from the TTR data analyzed with the three temperature model. The continued increase in measured h_{es} on the Au/glass samples demonstrates the temperature dependence of electron-interface scattering and how if affects h_{es}. The difference in the Au/Si and Au/glass trends shows the effect that the conductive Si substrate has on h_{es}. In the thinner samples, in which high electron temperatures are achieved during laser heating, scattering events around the film/substrate interface cause an increase in electron-phonon scattering. The effects of these scattering events are more pronounced on Si than glass due to the thermally conductive nature of Si, and therefore heat is more readily removed from the Au electron system.

difference between h_{es} measured on Au/Si and on Au/glass represents the rate at which electron energy is conducted across the film/Si interface. This analysis assumes that the differences in Au structure around the Au or Si and glass interfaces do not result in significantly different electron scattering rates. Also, note in Fig. 4 that as the trends in the Au/Si and Au/glass data decrease to a predicted electron temperature close to room temperature, the measured h_{es} approach values of $10-100$ MW m^{-2} K^{-1}, which is the same order of magnitude predicted by theoretical models for electron-substrate phonon scattering assuming a negligible electron-phonon nonequilibrium in the film.[61,62]

IV. CONCLUSIONS

Electron scattering at interfaces between metals and dielectrics is a major concern in thermal boundary conductance studies. This aspect of energy transfer has been extensively studied and modeled on long time scales when the electrons and phonons are in equilibrium in the metal film and when phonon-phonon interface scattering becomes a significant mode of boundary conductance. However, the effects of electron-substrate energy transfer have never been extensively considered in the event of an electron-phonon nonequilibrium, specifically, how this mode of energy transfer affects the electron cooling during equilibration. In this work, G in Au films of varying thicknesses was measured with the TTR technique. G is measured as much larger than predicted from traditional models. This increase in G increases as the film decreases in thickness and shows a substrate dependency, where G is measured as larger on a more conductive substrate. To explain this phenomenon, electron-substrate energy transfer during electron-phonon nonequilib-

rium is considered. The three temperature model is used to quantify electron-substrate boundary conductance obtained from fitting the three temperature model to the TTR data. The trends in the observed h_{es} suggest that electron equilibration can increase by interfacial scattering, which is substrate dependent.

ACKNOWLEDGMENTS

[1] A. N. Smith and J. P. Calame, Int. J. Thermophys. **25**, 409 (2004).
[2] R. C. Clarke and J. W. Palmour, Proc. IEEE **90**, 987 (2002).
[3] R. J. Trew, Proc. IEEE **90**, 1032 (2002).
[4] A. Majumdar, K. Fushinobu, and K. Hijikata, J. Appl. Phys. **77**, 6686 (1995).
[5] D. S. Ivanov and L. V. Zhigilei, Phys. Rev. B **68**, 064114 (2003).
[6] S.-S. Wellershoff, J. Hohlfeld, J. Gudde, and E. Matthias, Appl. Phys. A: Mater. Sci. Process. **69**, S99 (1999).
[7] S.-S. Wellershoff, J. Gudde, J. Hohlfeld, J. G. Muller, and E. Matthias, Proc. SPIE **3343**, 378 (1998).
[8] E. Beaurepaire, J.-C. Merle, A. Daunois, and J.-Y. Bigot, Phys. Rev. Lett. **76**, 4250 (1996).
[9] L. Guidoni, E. Beaurepaire, and J.-Y. Bigot, Phys. Rev. Lett. **89**, 017401 (2002).
[10] J. Hohlfeld, E. Matthias, R. Knorren, and K. H. Bennemann, Phys. Rev. Lett. **78**, 4861 (1997).
[11] B. Koopmans, M. van Kampen, J. T. Kohlhepp, and W. J. M. de Jonge, Appl. Phys. Lett. **87**, 5070 (2000).
[12] M. van Kampen, J. T. Kohlhepp, W. J. M. de Jonge, B. Koopmans, and R. Coehoorn, J. Phys.: Condens. Matter **17**, 6823 (2005).
[13] T. Q. Qiu, T. Juhasz, C. Suarez, W. E. Bron, and C. L. Tien, Int. J. Heat Mass Transfer **37**, 2799 (1994).
[14] T. Q. Qiu and C. L. Tien, Int. J. Heat Mass Transfer **37**, 2789 (1994).
[15] P. M. Norris, A. P. Caffrey, R. J. Stevens, J. M. Klopf, J. T. McLeskey, and A. N. Smith, Rev. Sci. Instrum. **74**, 400 (2003).
[16] J. Hohlfeld, S.-S. Wellershoff, J. Gudde, U. Conrad, V. Jahnke, and E. Matthias, Chem. Phys. **251**, 237 (2000).
[17] I. H. Chowdhury and X. Xu, Numer. Heat Transfer **44**, 219 (2003).
[18] T. Q. Qiu and C. L. Tien, ASME J. Heat Transfer **115**, 835 (1993).
[19] S. D. Brorson, J. G. Fujimoto, and E. P. Ippen, Phys. Rev. Lett. **59**, 1962 (1987).
[20] C. A. C. Bosco, A. Azevedo, and L. H. Acioli, Appl. Phys. Lett. **83**, 1767 (2003).
[21] T. Q. Qiu and C. L. Tien, ASME J. Heat Transfer **115**, 842 (1993).
[22] A. N. Smith, J. L. Hostetler, and P. M. Norris, Numer. Heat Transfer **35**, 859 (1999).
[23] G. V. Hartland, Int. J. Nanotechnol. **1**, 307 (2004).
[24] A. Arbouet, C. Voisin, D. Christofilos, P. Langot, N. Del Fatti, F. Vallee, J. Lerme, G. Celep, E. Cottancin, M. Gaudry, M. Pellarin, M. Broyer, M. Maillard, M. P. Pileni, and M. Treguer, Phys. Rev. Lett. **90**, 177401 (2003).
[25] J. H. Hodak, A. Henglein, and G. V. Hartland, J. Chem. Phys. **112**, 5942 (2000).
[26] A. N. Smith and P. M. Norris, Appl. Phys. Lett. **78**, 1240 (2001).
[27] P. E. Hopkins and P. M. Norris, Appl. Surf. Sci. **253**, 6289 (2007).
[28] P. E. Hopkins, J. M. Klopf, and P. M. Norris, Appl. Opt. **46**, 2076 (2007).
[29] Z. Lin, L. V. Zhigilei, and V. Celli, Phys. Rev. B **77**, 075133 (2008).
[30] S. I. Anisimov, B. L. Kapeliovich, and T. L. Perel'man, Sov. Phys. JETP **39**, 375 (1974).
[31] C. Kittel, *Introduction to Solid State Physics*, 7th ed. (Wiley, New York, 1996).
[32] J. L. Hostetler, A. N. Smith, D. M. Czajkowsky, and P. M. Norris, Appl. Opt. **38**, 3614 (1999).
[33] F. Incropera and D. P. DeWitt, *Fundamentals of Heat and Mass Transfer*, 4th ed. (Wiley, New York, 1996).
[34] S. I. Anisimov and B. Rethfeld, Proc. SPIE **3093**, 192 (1997).
[35] J. Hohlfeld, J. G. Muller, S.-S. Wellershoff, and E. Matthias, Appl. Phys. B: Lasers Opt. **64**, 387 (1997).
[36] A. P. Caffrey, P. E. Hopkins, J. M. Klopf, and P. M. Norris, Microscale Thermophys. Eng. **9**, 365 (2005).
[37] A. H. MacDonald, Phys. Rev. Lett. **44**, 489 (1980).
[38] N. W. Ashcroft and N. D. Mermin, *Solid State Physics* (Saunders College, Fort Worth, 1976).
[39] R. Rosei and D. W. Lynch, Phys. Rev. B **5**, 3883 (1972).
[40] S. D. Brorson, A. Kazeroonian, J. S. Moodera, D. W. Face, T. K. Cheng, E. P. Ippen, M. S. Dresselhaus, and G. Dresselhaus, Phys. Rev. Lett. **64**, 2172 (1990).
[41] H. Hirori, T. Tachizaki, O. Matsuda, and O. B. Wright, Phys. Rev. B **68**, 113102 (2003).
[42] W. J. Scouler, Phys. Rev. Lett. **18**, 445 (1967).
[43] G. L. Eesley, Phys. Rev. B **33**, 2144 (1986).
[44] E. Colavita, A. Franciosi, C. Mariani, and R. Rosei, Phys. Rev. B **27**, 4684 (1983).
[45] J. Hanus, J. Feinleib, and W. J. Scouler, Phys. Rev. Lett. **19**, 16 (1967).
[46] H. Ehrenreich and H. R. Philipp, Phys. Rev. **128**, 1622 (1962).
[47] H. Ehrenreich, H. R. Philipp, and B. Segall, Phys. Rev. **132**, 1918 (1963).
[48] R. Hummel, *Electronic Properties of Materials*, 2nd ed. (Springer, New York, 1997).
[49] M. I. Markovic and A. D. Rakic, Appl. Opt. **29**, 3479 (1990).
[50] M. I. Markovic and A. D. Rakic, Opt. Laser Technol. **22**, 394 (1990).
[51] J. M. Ziman, *Electrons and Phonons* (Clarendon, Oxford, 1960).
[52] G. Laufer, *Introduction to Optics and Lasers in Engineering* (Cambridge University Press, Cambridge, 1996).
[53] E. D. Palik, *Handbook of Optical Constants of Solids* (Academic, Orlando, 1985).
[54] F. Abeles, in *Advanced Optical Techniques*, edited by A. C. S. V. Heel (North-Holland, Amsterdam, 1967), pp. 145–188.
[55] D. E. Gray, *American Institute of Physics Handbook*, 3rd ed. (McGraw-Hill, New York, 1972).
[56] X. Y. Wang, D. M. Riffe, Y.-S. Lee, and M. C. Downer, Phys. Rev. B **50**, 8016 (1994).
[57] M. Kaveh and N. Wiser, Adv. Phys. **33**, 257 (1984).
[58] R. J. Stevens, A. N. Smith, and P. M. Norris, Rev. Sci. Instrum. **77**, 084901 (2006).
[59] W. G. Vincenti and C. H. Kruger, *Introduction to Physical Gas Dynamics* (Krieger, Malabar, FL, 2002).
[60] J. K. Chen, W. P. Latham, and J. E. Beraun, J. Laser Appl. **17**, 63 (2005).
[61] A. V. Sergeev, Phys. Rev. B **58**, R10199 (1998).
[62] A. V. Sergeev, Physica B **263–264**, 217 (1999).